Constraint preserving schemes using potential-based fluxes

I. Multidimensional transport equations

S. Mishra and E. Tadmor[*]

---

[*]Department of Mathematics, Institute for Physical Sciences and Technology (IPST), University of Maryland, College Park, MD 20742-4015, USA

CONSTRAINT PRESERVING SCHEMES USING POTENTIAL-BASED FLUXES. I. MULTIDIMENSIONAL TRANSPORT EQUATIONS

SIDDHARTHA MISHRA AND EITAN TADMOR

To the memory of David Gottlieb

ABSTRACT. We consider constraint preserving multidimensional evolution equations. A prototypical example is provided by the magnetic induction equation of plasma physics. The constraint of interest is the divergence of the magnetic field. We design finite volume schemes which approximate these equations in a stable manner and preserve a discrete version of the constraint. The schemes are based on reformulating standard edge centered finite volume fluxes in terms of vertex centered potentials. The *potential-based* approach provides a general framework for faithful discretizations of constraint transport and we apply it to both divergence preserving as well as curl preserving equations. We present benchmark numerical tests which confirm that our potential-based schemes achieve high resolution, while being constraint preserving.

1. INTRODUCTION

We are concerned with evolution equations of the form

$$(1.1) \qquad \mathbf{u}_t + L(\partial_x, \mathbf{f}(x, t, \mathbf{u})) = 0, \quad \forall (x, t) \in \mathbb{R}^n \times \mathbb{R}_+,$$

where $\mathbf{u}(x, t) : \mathbb{R}^n \times \mathbb{R}_+ \mapsto \mathbb{R}^m$ is the unknown, $\mathbf{f} : X \mapsto X$ is a nonlinear flux function and $L : X \mapsto Y$ is a differential operator acting on the Sobolev space X. We assume there exists another differential operator $M : Y \mapsto Z$ such that $ML(\mathbf{f}(\cdot, \cdot, \mathbf{v})) \equiv 0$ for all $\mathbf{v} \in X$. Applying the operator M to both sides of (1.1), we obtain

$$(1.2) \qquad (M\mathbf{u})_t \equiv 0.$$

Hence, solutions of (1.1) satisfy an additional constraint which enforces them to lie on a sub-manifold of the space X.

The above framework is generic to a large class of evolution equations involving *intrinsic constraints*. We mention three prototype examples. As a first example, consider the curl advection:

$$(1.3) \qquad \mathbf{u}_t + \operatorname{curl}(\mathbf{f}(x, t, \mathbf{u})) = 0, \quad (x, t) \in \mathbb{R}^n \times R_+.$$

This equation is an example for (1.1),(1.2) with the differential operators $L = \operatorname{curl}$ and $M = \operatorname{div}$. Hence, solutions of (1.3) satisfy the additional divergence constraint:

$$(1.4) \qquad \operatorname{div}(\mathbf{u})_t = 0.$$

A specific example for (1.3) is the magnetic induction equation of plasma physics. Under the assumptions of zero resistivity, the magnetic field $\mathbf{u}$, evolving under the influence of a given velocity $\mathbf{v}$, satisfies the following form of the Maxwell's equations [23]:

$$(1.5) \qquad \mathbf{u}_t + \operatorname{curl}(\mathbf{u} \times \mathbf{v}) = 0, \quad (x, t) \in \mathbb{R}^n \times \mathbb{R}_+.$$

The fact that magnetic monopoles have not been observed in nature implies that

$$\text{(1.6)} \qquad\qquad\qquad\qquad \text{div}(\mathbf{u}(x,0)) \equiv 0.$$

As a consequence of the divergence constraint (1.4), the solutions of (1.5) remain divergence free. The magnetic induction equation (1.5) is a sub-model for the equations of ideal Magnetohydrodynamics (MHD) [11].

Adding magnetic resistivity to the model leads to the viscous magnetic induction equations:

$$\text{(1.7)} \qquad\qquad \mathbf{u}_t + \text{curl}(\mathbf{u} \times \mathbf{v}) = -\sigma(\text{curl}(\text{curl}\mathbf{u})), \quad (x,t) \in \mathbb{R}^n \times \mathbb{R}_+.$$

The parameter σ is the resistivity co-efficient of the medium. Solutions of (1.7) also satisfy the divergence constraint (1.4).

A second example for (1.1),(1.2) is the grad advection:

$$\text{(1.8)} \qquad\qquad \mathbf{w}_t + \text{grad}(\mathbf{f}(x,t,\mathbf{w})) = 0, \quad (x,t) \in \mathbb{R}^n \times \mathbb{R}_+.$$

The differential operators of interest are $L = \text{grad}$ and $M = \text{curl}$ and solutions of (1.8) satisfy the additional constraint,

$$\text{curl}(\mathbf{w})_t = 0.$$

A related example is the system of two dimensional linear wave equations [21]:

$$\text{(1.9)} \qquad\qquad \begin{cases} p_t + cu_x + cv_y = 0, \\ u_t + cp_x = 0, \\ v_t + cp_y = 0. \end{cases}$$

The corresponding differential operators L and M are

$$L = \begin{pmatrix} 0 & c & 0 \\ c & 0 & 0 \\ 0 & 0 & 0 \end{pmatrix} \partial_x + \begin{pmatrix} 0 & 0 & c \\ 0 & 0 & 0 \\ c & 0 & 0 \end{pmatrix} \partial_y,$$

and $M = (0,0,1)\,\partial_x + (0,-1,0)\,\partial_y$ picks the vorticity of the flow, $\omega := v_x - u_y$.

A third – considerably more complicated example of evolution equations with *non-linear* constraints is provided by the Einstein equations [10].

Standard finite volume/finite difference numerical schemes for approximating (1.1),(1.2) may not necessarily treat the constraint properly and may fail to be stable [11]. Hence, suitable *constraint preserving* schemes need to be devised for robust approximation of (1.1),(1.2). Design of efficient numerical schemes for the constrained evolution equations (1.1),(1.2) is a highly active research area, consult [1, 9, 21, 24, 31] and references therein. We mention below three main methods available in the literature for handling constraint transport equations, where most of the attention is devoted to applications to the ideal MHD and the magnetic induction equations (1.5).

1.1. **Projection method.** This method [7, 6, 5] is based on the Hodge decomposition of the solution $\mathbf{u}$ of (1.5). The update $\mathbf{u}^n$ at each time step may not be divergence free and is corrected by the decomposition, $\mathbf{u}^n = \nabla\Psi + \text{curl}\Phi$. Applying the divergence operator to the Hodge decomposition leads to the elliptic equation:

$$-\Delta\Psi = \text{div}(\mathbf{u}^n).$$

The corrected field $\mathbf{u}^* = \mathbf{u}^n - \nabla\Psi$ is divergence free. This method can be very expensive computationally as an elliptic equation has to be solved at every time step, augmented with proper set of boundary conditions, e.g. [31].

1.2. **Source terms.** Adding a source term proportional to the divergence in (1.5) results in

$$\text{(1.10)} \qquad\qquad \mathbf{u}_t + \text{curl}(\mathbf{u} \times \mathbf{v}) = -\mathbf{v}\text{div}(\mathbf{u}).$$

Applying the divergence to both sides, we obtain

$$(\text{div}(\mathbf{u}))_t + \text{div}(\mathbf{v}\text{div}\mathbf{u}) = 0.$$

Hence, any potential divergence errors are transported away from the computational domain by the flow. Furthermore, the form (1.10) is symmetrizable [13]. This procedure for "cleaning" the divergence was introduced

in [22, 23]. Recent papers [11, 12] have demonstrated that the source term in (1.10) needs to be discretized in a very careful manner for numerical stability. Another problem with this approach lies in the non-conservative form of (1.10). Hence, numerical schemes based on this approach may result in wrong shock speeds [31].

1.3. **Design of special divergence operators/staggering.** This popular method consists of staggering the discretizations of the velocity and magnetic fields in (1.5). A wide variety of strategies for staggering the meshes has been proposed [9, 4, 8, 24, 31, 3, 2] and references therein. The presence of different sets of meshes leads to problems when the staggered schemes are parallelized. Unstaggered variants of this approach have also been proposed in [30, 29, 1]. The approach suggested in [30] is of particular relevance for this paper; the authors suggest an unstaggered method, based on *upwinded flux distributions* in each cell, resulting in a scheme which preserves a particular discrete form of divergence.

The above examples leave room for designing other *constraint preserving schemes* that are easy to implement and computationally robust. In this paper we propose a new approach for designing such schemes. Our starting point is the *genuinely multi-dimensional* structure of equation (1.1) complemented with the constraint (1.2). This is in contrast to standard finite volume schemes based on locally one dimensional edge centered fluxes [18, 28], which do not incorporate any explicit information in the transverse direction. Here, we introduce a new approach to modify standard finite volume schemes which incorporates genuinely multi-dimensional information, resulting in a new family of constraint preserving schemes.

To this end, we propose the construction of vertex-centered *numerical potentials* which serve as the building blocks of our constraint preserving schemes. Written in terms of these numerical potentials, the proposed schemes are genuinely multi-dimensional and preserve a discrete form of the constraint (1.2). The framework is very general, easy to code and allow for *any* consistent numerical flux to be used as a building block for the construction of numerical potentials. No additional upwinding is necessary for numerical stability. Our new, so-called *potential-based* approach, is demonstrated in the context of the linear magnetic induction equation (1.5). The potential-based schemes preserve a discrete version of divergence. We prove numerical stability for certain versions of these schemes. Numerical experiments illustrating the generality of the approach and its computational efficiency are presented.

The rest of this paper is organized as follows: in section 2, we describe the general form of constraint preserving potential-based schemes. In section 3, the magnetic induction equation (1.5) are considered and some stability results presented. Numerical experiments are presented in section 4. This paper is the first in a series of papers devoted to genuinely multi-dimensional schemes based on numerical potentials. Subsequent papers, [19, 20], will extend this approach to non-linear conservation laws, including the equations of MHD.

2. Potential based Constraint preserving schemes

For simplicity of the exposition, we start with the two dimensional form of *curl* advection (1.3):

$$
(2.1) \qquad \begin{cases} (u_1)_t + f_y = 0, \\ (u_2)_t - f_x = 0, \end{cases}
$$

with the flux $f = f(x, y, t, \mathbf{u})$, where $\mathbf{u} := (u_1, u_2)$ is the 2-vector of unknowns subject to divergence-free initial condition $\operatorname{div} \mathbf{u}(x, y, 0) = 0$.

We consider a uniform Cartesian mesh with mesh sizes $\Delta x, \Delta y$ in the x- and y- directions respectively. It consists of the discrete cells, $\mathcal{C}_{i,j} = [x_{i-\frac{1}{2}}, x_{i+\frac{1}{2}}) \times [y_{j-\frac{1}{2}}, y_{j+\frac{1}{2}})$, centered at the mesh points $(x_i, y_j) = (i\Delta x, j\Delta y)$, $(i, j) \in \mathbb{Z}^2$. To approximate (2.1), we use standard discrete averaging and difference operators

$$
(2.2) \qquad \begin{aligned} \mu_x a_{I,J} &:= \frac{a_{I+\frac{1}{2},J} + a_{I-\frac{1}{2},J}}{2}, \quad \mu_y a_{I,J} := \frac{a_{I,J+\frac{1}{2}} + a_{I,J-\frac{1}{2}}}{2}, \\ \delta_x a_{I,J} &:= a_{I+\frac{1}{2},J} - a_{I-\frac{1}{2},J}, \quad \delta_y a_{I,J} := a_{I,J+\frac{1}{2}} - a_{I,J-\frac{1}{2}}. \end{aligned}
$$

A word about our notations: we note that the above discrete operators could be used with indexes I, J which are placed at the center or at the edge of the computational cells, e.g., $I = i$ or $I = i + \frac{1}{2}$. In either case, we tag the resulting discrete operators according to the center of their stencil; thus, for example, $\mu_x w_{i+\frac{1}{2}}$ employs

gridvalues placed on the integer-indexed edges, w_i and w_{i+1}, whereas $\delta_y w_j$ employs the half-integer indexed centers, $w_{j\pm\frac{1}{2}}$.

A standard semi-discrete finite volume scheme [18, 28] for updating the cell averages $\mathbf{u}_{i,j}(t)$ in (2.1) at time t can be expressed as (dropping t for notational convenience)

$$(2.3) \qquad \begin{aligned} \frac{d}{dt}(u_1)_{i,j} &= -\frac{1}{\Delta y}\delta_y F^y_{i,j} \equiv -\frac{1}{\Delta y}\left(F^y_{i,j+\frac{1}{2}} - F^y_{i,j-\frac{1}{2}}\right), \\ \frac{d}{dt}(u_2)_{i,j} &= \frac{1}{\Delta x}\delta_x F^x_{i,j} \equiv \frac{1}{\Delta x}\left(F^x_{i+\frac{1}{2},j} - F^x_{i-\frac{1}{2},j}\right), \end{aligned}$$

where $F^x_{i+\frac{1}{2},j}$ and $F^y_{i,j+\frac{1}{2}}$ are edge centered numerical fluxes, consistent with the flux f in the x- and y- directions respectively. Examples for numerical fluxes include fluxes in the viscosity form [26]:

$$(2.4) \qquad \begin{aligned} F^x_{i+\frac{1}{2},j} &= \mu_x f_{i+\frac{1}{2},j} + Q^x_{i+\frac{1}{2},j}\delta_x(u_2)_{i+\frac{1}{2},j}, \\ F^y_{i,j+\frac{1}{2}} &= \mu_y f_{i,j+\frac{1}{2}} - Q^y_{i,j+\frac{1}{2}}\delta_y(u_1)_{i,j+\frac{1}{2}}, \end{aligned}$$

where $f_{i,j} := f(x_i, y_j, t, \mathbf{u}_{i,j})$ and $Q^x = Q^x(x,y,t,\mathbf{u})$ and $Q^y = Q^y(x,y,t,\mathbf{u})$ are suitable numerical viscosity coefficients. For example, the first-order Rusanov flux for (2.1) has the viscosity form (2.4) with viscosity coefficients

$$(2.5a) \qquad Q^x_{i+\frac{1}{2},j} = \max\left\{|\lambda^{(2)}_{i,j}|, |\lambda^{(2)}_{i+1,j}|\right\}, \qquad Q^y_{i,j+\frac{1}{2}} = \max\left\{|\lambda^{(1)}_{i,j}|, |\lambda^{(1)}_{i,j+1}|\right\},$$

where $\lambda^{(\ell)}$ are the eigenvalues of the corresponding Jacobians,

$$(2.5b) \qquad |\lambda^{(\ell)}_{i,j}| = \left|\frac{\partial f}{\partial u_\ell}(x_i, y_j, t, \mathbf{u}_{i,j})\right|, \quad \ell = 1, 2.$$

The family of viscous numerical fluxes (2.4) will be shown to serve as building blocks for the potential-based schemes discussed in section 2.1 below.

The standard finite volume scheme (2.3) may not preserve any discrete form of the divergence constraint (1.4) [11], which in turn may lead to numerical instabilities. To address this difficulty, we introduce a family of genuinely multi-dimensional schemes based on *numerical potentials* $\phi_{i+\frac{1}{2},j+\frac{1}{2}}$, defined at vertices $x_{i+\frac{1}{2}}, y_{j+\frac{1}{2}}$ with the sole requirement that these potentials are consistent with the differential flux,

$$(2.6) \qquad \phi(x, y, t, \mathbf{u}, \cdots, \mathbf{u}) = f(x, y, t, \mathbf{u}).$$

We now set the numerical fluxes

$$\begin{aligned} F^x_{i,j+\frac{1}{2}} &= \mu_x \phi_{i,j+\frac{1}{2}}, \\ F^y_{i+\frac{1}{2},j} &= \mu_y \phi_{i+\frac{1}{2},j}. \end{aligned}$$

The resulting finite volume scheme written in terms of numerical potentials reads

$$(2.7) \qquad \begin{aligned} \frac{d}{dt}(u_1)_{i,j} &= -\frac{1}{\Delta y}\delta_y \mu_x \phi_{i,j} \equiv -\frac{1}{\Delta y}\left(\frac{1}{2}\left(\phi_{i+\frac{1}{2},j+\frac{1}{2}} + \phi_{i-\frac{1}{2},j+\frac{1}{2}}\right) - \frac{1}{2}\left(\phi_{i+\frac{1}{2},j-\frac{1}{2}} + \phi_{i-\frac{1}{2},j-\frac{1}{2}}\right)\right), \\ \frac{d}{dt}(u_2)_{i,j} &= \frac{1}{\Delta x}\delta_x \mu_y \phi_{i,j} \equiv \frac{1}{\Delta x}\left(\frac{1}{2}\left(\phi_{i+\frac{1}{2},j+\frac{1}{2}} + \phi_{i+\frac{1}{2},j-\frac{1}{2}}\right) - \frac{1}{2}\left(\phi_{i-\frac{1}{2},j+\frac{1}{2}} + \phi_{i-\frac{1}{2},j-\frac{1}{2}}\right)\right). \end{aligned}$$

The scheme (2.7) is consistent with (2.1) since the numerical potential is. There is a remarkably rich family of consistent potential-based schemes — a host of examples will be specified in the next subsection. They have a genuinely multi-dimensional structure, due to the vertex-centered numerical potentials which include information in both normal as well as transverse directions. Observe that the potential-based scheme need not involve any staggering of meshes. But before turning to specific examples of potential-based schemes we describe their main motivation in the present context of divergence-free equations.

Lemma 2.1. *Let $\mathbf{u}_{i,j}$ be the numerical solution of the potential-based scheme (2.7),(2.6). Then, their discrete divergence, div^*, given by*

$$(2.8a) \qquad \mathrm{div}^*(\mathbf{u}_{i,j}) := \frac{1}{\Delta x}\mu_y \delta_x(u_1)_{i,j} + \frac{1}{\Delta y}\mu_x \delta_y(u_2)_{i,j},$$

is preserved in time:

(2.8b)
$$\frac{d}{dt}\text{div}^*(\mathbf{u}_{i,j}) \equiv 0, \quad \forall i, j.$$

Verification of (2.8b) is straightforward: since the difference operators δ_x, δ_y and the averaging operators μ_x, μ_y commute with each other, applying the discrete divergence operator div^* to the numerical solution of (2.7) we find

$$\frac{d}{dt}\text{div}^*(\mathbf{u}_{i,j}) = -\frac{1}{\Delta x \Delta y}(\mu_y \delta_x \delta_y \mu_x - \mu_x \delta_y \delta_x \mu_y)\phi_{i,j} \equiv 0.$$

Remark 2.1. *One approach in designing constraint preserving schemes is to satisfy that constraint* approximately*: for example, the discrete statement of* (2.8a) *could be interpreted as a second-order approximation of the differential divergence,*

$$\text{div}^*(\mathbf{u}_{i,j}) = \text{div }\mathbf{u}(x_i, y_j) + \mathcal{O}(\Delta x^2 + \Delta y^2).$$

This, however, requires the smoothness of the underlying solution. Instead, a key feature of constraint preserving schemes based on numerical potentials is that they satisfy exactly *a discrete constraint, so that their numerical solution remains on a discrete sub-manifold, independent of the underlying smoothness.*

Lemma 2.1 shows that the class of potential-based schemes satisfies a precise discrete analogue of the divergence constraint (1.4). We emphasize that it applies to *any* consistent numerical potential. Special cases of the discrete divergence operator div^* (2.8a) were considered in [30, 29]. This level of generality of the potential-based approach offers a major advantage over earlier studies, and is explored next.

2.1. **The family of potential-based schemes is rich.** Numerical potentials ϕ in (2.7) can be chosen in many different ways. The examples below illustrate the generality of our potential-based approach.

2.1.1. *Symmetric potential.* A consistent choice of potential ϕ is obtained by averaging neighboring edge centered fluxes, i.e,

(2.9)
$$\phi_{i+\frac{1}{2},j+\frac{1}{2}} = \frac{1}{4}\left(F^x_{i+\frac{1}{2},j} + F^x_{i+\frac{1}{2},j+1} + F^y_{i,j+\frac{1}{2}} + F^y_{i+1,j+\frac{1}{2}}\right),$$

where $F^x_{i+\frac{1}{2},j}, F^y_{i,j+\frac{1}{2}}$ are consistent numerical fluxes. Higher order fluxes can be readily used.

An explicit computation of the scheme (2.7) with the symmetric potentials (2.9) leads to the revealing form,

(2.10)
$$\frac{d}{dt}(u_1)_{i,j} = -\frac{1}{4\Delta y}\left(\mu_x F^x_{i,j+1} - \mu_x F^x_{i,j-1}\right) - \frac{1}{4\Delta y}\left(\delta_y(\mu_x F^y_{i+1/2,j} + \mu_x F^y_{i-1/2,j})\right),$$
$$\frac{d}{dt}(u_2)_{i,j} = \frac{1}{4\Delta x}\left(\mu_y F^y_{i+1,j} - \mu_y F^y_{i-1,j}\right) + \frac{1}{4\Delta x}\left(\delta_x(\mu_y F^x_{i,j+1/2} + \mu_x F^x_{i,j-1/2})\right).$$

The above form suggests that the potential based scheme (2.7) introduces a special *transverse* correction (by averaging normal fluxes in the transverse direction) to the standard finite volume scheme (2.3). The above form brings out the contrast between the standard finite volume scheme (2.3) and the potential based scheme (2.7) quite sharply.

2.1.2. *Staggered symmetric potential.* A different consistent potential can be defined as

(2.11)
$$\phi_{i+\frac{1}{2},j+\frac{1}{2}} = \frac{1}{2}\left(F^x\left(\mu_y \mathbf{u}_{i,j+\frac{1}{2}}, \mu_y \mathbf{u}_{i+1,j+\frac{1}{2}}\right) + F^y\left(\mu_x \mathbf{u}_{i+\frac{1}{2},j}, \mu_x \mathbf{u}_{i+\frac{1}{2},j+1}\right)\right),$$

where F^x, F^y are consistent two-point numerical fluxes. This approach is equivalent to the symmetric potential (2.9) for linear equations with constant coefficients. However, it leads to a different scheme for equations with variable coefficients and for equations with non-linear fluxes.

2.1.3. *Diagonal Potential.* A completely different form of the potential is defined by

$$\phi_{i+\frac{1}{2},j+\frac{1}{2}} = \frac{1}{2}\Big(F^x(\mathbf{u}_{i,j},\mathbf{u}_{i+1,j+1}) + F^y(\mathbf{u}_{i,j},\mathbf{u}_{i+1,j+1})\Big), \tag{2.12}$$

where F^x and F^y are consistent two-point numerical fluxes. It is straightforward to extend this form for any $2k$-point numerical fluxes. This form of the potential is *isotropic* and leads to a compact form of the scheme (2.7).

2.1.4. *Mixed Potential.* A slightly different form of the diagonal potential is obtained as,

$$\phi_{i+\frac{1}{2},j+\frac{1}{2}} =$$
$$= \frac{1}{4}\Big(F^x(\mathbf{u}_{i,j},\mathbf{u}_{i+1,j+1}) + F^x(\mathbf{u}_{i,j+1},\mathbf{u}_{i+1,j}) + F^y(\mathbf{u}_{i+1,j},\mathbf{u}_{i,j+1}) + F^y(\mathbf{u}_{i,j},\mathbf{u}_{i+1,j+1})\Big), \tag{2.13}$$

where F^x, F^y are consistent two-point numerical fluxes.

2.2. **Second order potential-based schemes.** The order of accuracy of the scheme (2.7) is related to the choice of numerical fluxes F^x, F^y used to define the potentials. The discrete divergence operator div* (2.8a) and the difference and averaging operators (2.2) are second-order accurate. Therefore, overall second-order spatial accuracy is obtained by using standard non-oscillatory piecewise linear reconstructions in each cell. We follow the reconstruction procedure proposed in [17].

2.2.1. *Second order non-oscillatory reconstruction.* The cell averages $\mathbf{u}_{i,j}$ are used to define the piecewise bilinear reconstruction,

$$\mathbf{p}_{i,j}(x,y) = \mathbf{u}_{i,j} + \frac{\mathbf{u}'_{i,j}}{\Delta x}(x - x_i) + \frac{\mathbf{u}^{\backprime}_{i,j}}{\Delta y}(y - y_j), \tag{2.14a}$$

The numerical derivatives in $x-$ and $y-$ directions, denoted respectively by prime and backprime are given by the standard limiter,

$$\mathbf{u}'_{i,j} = \mathrm{minmod}(\mathbf{u}_{i+1,j} - \mathbf{u}_{i,j}, 0.5(\mathbf{u}_{i+1,j} - \mathbf{u}_{i-1,j}), \mathbf{u}_{i,j} - \mathbf{u}_{i-1,j}),$$
$$\mathbf{u}^{\backprime}_{i,j} = \mathrm{minmod}(\mathbf{u}_{i,j+1} - \mathbf{u}_{i,j}, 0.5(\mathbf{u}_{i,j+1} - \mathbf{u}_{i,j-1}), \mathbf{u}_{i,j} - \mathbf{u}_{i,j-1}). \tag{2.14b}$$

The minmod function, defined as

$$\mathrm{minmod}(a,b,c) := \begin{cases} sgn(a)\min\{|a|,|b|,|c|\}, & \text{if } sgn(a) = sgn(b) = sgn(c), \\ 0, & \text{otherwise,} \end{cases}$$

is a standard van-Leer limiter; other standard limiters can also be used in this context. The use of limiters ensures that the reconstruction of each unknown is non-oscillatory e.g., total-variation diminishing, consult [28] and the references therein. In the sequel, we will also need the following reconstructed corner pointvalues,

$$\mathbf{u}^E_{i,j} = \mathbf{p}_{i,j}(x_{i+\frac{1}{2}}, y_j), \quad \mathbf{u}^W_{i,j} = \mathbf{p}_{i,j}(x_{i-\frac{1}{2}}, y_j),$$
$$\mathbf{u}^N_{i,j} = \mathbf{p}_{i,j}(x_i, y_{j+\frac{1}{2}}), \quad \mathbf{u}^S_{i,j} = \mathbf{p}_{i,j}(x_i, y_{j-\frac{1}{2}}). \tag{2.14c}$$

Given the any consistent two-point fluxes F, G , a second order flux based on a midpoint rule to compute edge integrals takes the from,

$$F^x_{i+\frac{1}{2},j} = F^x(\mathbf{u}^E_{i,j}, \mathbf{u}^W_{i+1,j}), \quad F^y_{i,j+\frac{1}{2}} = F^y(\mathbf{u}^N_{i,j}, \mathbf{u}^S_{i,j+1}). \tag{2.14d}$$

The above fluxes are used to define the potentials in the scheme (2.7) resulting in an overall second order accurate discretization of (2.1).

Remark 2.2. *In order to achieve third and even higher order accuracy in space, we need to redefine the averaging and difference operators given in (2.7) to higher than second order accuracy. The potentials can then be expressed in form of fluxes, based on third and even higher order (W)ENO type reconstructions, [15, 25]. This program for designing schemes of arbitrary orders of accuracy will be considered in a forthcoming paper.*

2.3. **A divergence preserving viscous discretization.** The two dimensional form of the divergence preserving viscous equation (1.7) is

$$(2.15) \qquad \begin{cases} (u_1)_t + f_y = (u_1)_{yy} - (u_2)_{xy}, \\ (u_2)_t - f_x = (u_2)_{xx} - (u_1)_{xy}. \end{cases}$$

Note that the viscosity in (2.15) is of the curl(curl) type.

We combine the potential based discretization of the flux terms in (2.1) with a simple genuinely multi-dimensional discretization of the viscous term to obtain a divergence preserving scheme for (2.15). Below, we employ the standard notations for forward, backward and centered divided differences,

$$D_x^{\pm} a_{i,j} = \frac{\pm(a_{i\pm1,j} - a_{i,j})}{\Delta x}, \quad D_y^{\pm} a_{i,j} = \frac{\pm(a_{i,j\pm1} - a_{i,j})}{\Delta y}, \quad D_{x,y}^0 a_{i,j} = \frac{D_{x,y}^+ a_{i,j} + D_{x,y}^- a_{i,j}}{2}.$$

The divergence preserving scheme for (2.1) is

$$(2.16) \qquad \begin{aligned} \frac{d}{dt}(u_1)_{i,j} &= -\frac{1}{\Delta y}\delta_y\mu_x\phi_{i,j} - D_x^0 D_y^0 (u_2)_{i,j} \\ &\quad + \frac{1}{4}\left(D_y^+ D_y^- (u_1)_{i+1,j} + 2D_y^+ D_y^- (u_1)_{i,j} + D_y^+ D_y^- (u_1)_{i-1,j}\right), \\ \frac{d}{dt}(u_2)_{i,j} &= \frac{1}{\Delta x}\delta_x\mu_y\phi_{i,j} - D_x^0 D_y^0 (u_1)_{i,j} \\ &\quad + \frac{1}{4}\left(D_x^+ D_x^- (u_2)_{i,j+1} + 2D_x^+ D_x^- (u_2)_{i,j} + D_x^+ D_x^- (u_2)_{i,j-1}\right). \end{aligned}$$

The above scheme is a consistent discretization of (2.15). A straightforward calculation, together with Lemma 2.1 shows that the scheme (2.16) preserves the discrete divergence operator div*. Note that the viscous terms are discretized in a genuinely multi-dimensional manner in (2.16).

2.4. **Curl preserving discretization.** The g*rad* advection equation (1.8) in two space dimensions with flux $f = f(x, y, t, \mathbf{u})$ is given by

$$(2.17) \qquad \begin{cases} (u_1)_t + f_x = 0, \\ (u_2)_t + f_y = 0. \end{cases}$$

We follow the strategy of the previous sections, seeking a consistent vertex centered potential, $\phi_{i+\frac{1}{2},j+\frac{1}{2}}$. The corresponding potential-based scheme reads

$$(2.18) \qquad \begin{aligned} \frac{d}{dt}(u_1)_{i,j} &= -\frac{1}{\Delta x}\delta_x\mu_y\phi_{i,j}, \\ \frac{d}{dt}(u_2)_{i,j} &= -\frac{1}{\Delta y}\delta_y\mu_x\phi_{i,j}, \end{aligned}$$

The scheme preserves the following discrete curl operator,

$$(2.19) \qquad \frac{d}{dt}\mathrm{curl}^*(\mathbf{u}_{i,j}) \equiv 0, \qquad \mathrm{curl}^*(\mathbf{u}_{i,j}) = \frac{1}{\Delta x}\mu_x\delta_y(u_1)_{i,j} - \frac{1}{\Delta y}\mu_y\delta_x(u_2)_{i,j}.$$

The proof follows along the lines of lemma (2.1). The potentials can be defined in a manner, analogous to the divergence preserving scheme (2.7). Indeed, the two-dimensional divergence and curl preserving equations, (2.1) and (2.17), and their corresponding potential-based schemes, (2.7) and (2.18), are dual to each other.

2.5. **Divergence preserving schemes in three dimensions.** The three dimensional divergence preserving equations (1.3) with flux vector $\mathbf{f} = (f_1, f_2, f_3)$, are explicitly written as,

$$(2.20) \qquad \begin{aligned} (u_1)_t + (f_3)_y - (f_2)_z &= 0, \\ (u_2)_t + (f_1)_z - (f_3)_x &= 0, \\ (u_3)_t + (f_2)_x - (f_1)_y &= 0, \end{aligned}$$

It is straightforward to extend the potential based framework of this section and design a divergence preserving scheme for the above equation. Let δ_x, δ_y and δ_z, μ_x, μ_y and μ_z denote the difference and average operators in the x, y and z directions respectively. Define a uniform grid in all three directions $(x_i, y_j, z_k) = (i\Delta x, j\Delta y, k\Delta z)$ with mesh sizes $\Delta x, \Delta y$ and Δz. Also, denote the cell $\mathcal{C}_{i,j,k} = [x_{i-\frac{1}{2}}, x_{i+\frac{1}{2}}) \times [y_{j-\frac{1}{2}}, y_{j+\frac{1}{2}}) \times [z_{k-\frac{1}{2}}, z_{k+\frac{1}{2}})$ and the cell average of the unknown over the cell $\mathcal{C}_{i,j,k}$ as $\mathbf{u}_{i,j,k}$.

We need to define three vertex centered potentials $(\phi_l)_{i+\frac{1}{2}, j+\frac{1}{2}, k+\frac{1}{2}}$ with $l = 1, 2, 3$, such that they are consistent , i.e,

$$(2.21) \qquad (\phi_l)_{i+\frac{1}{2}, j+\frac{1}{2}, k+\frac{1}{2}}(x, y, z, t, \mathbf{u}, \cdots, \mathbf{u}) = f_l(\mathbf{u}), \qquad l = 1, 2, 3.$$

The divergence preserving scheme in three dimensions is defined in terms of the potentials as

$$(2.22) \qquad \begin{aligned} \frac{d}{dt}(u_1)_{i,j,k} &= -\frac{1}{\Delta y}\delta_y\mu_x\mu_z(\phi_3)_{i,j,k} + \frac{1}{\Delta z}\delta_z\mu_x\mu_y(\phi_2)_{i,j,k}, \\ \frac{d}{dt}(u_2)_{i,j,k} &= -\frac{1}{\Delta z}\delta_z\mu_x\mu_y(\phi_1)_{i,j,k} + \frac{1}{\Delta x}\delta_x\mu_y\mu_z(\phi_3)_{i,j,k}, \\ \frac{d}{dt}(u_3)_{i,j,k} &= -\frac{1}{\Delta x}\delta_x\mu_y\mu_z(\phi_2)_{i,j,k} + \frac{1}{\Delta y}\delta_y\mu_x\mu_z(\phi_1)_{i,j,k}. \end{aligned}$$

Arguing along the lines of lemma 2.1 we now state the following divergence preserving property.

Lemma 2.2. *Let $\mathbf{u}_{i,j,k}$ be the numerical solution of the potential-based scheme* (2.22),(2.21). *Then, their discrete divergence,* div^*, *given by*

$$(2.23a) \qquad \mathrm{div}^*(\mathbf{u}_{i,j,k}) = \frac{1}{\Delta x}\mu_y\mu_z\delta_x(u_1)_{i,j,k} + \frac{1}{\Delta y}\mu_x\mu_z\delta_y(u_2)_{i,j,k} + \frac{1}{\Delta z}\mu_y\mu_x\delta_z(u_3)_{i,j,k},$$

is preserved in time:

$$(2.23b) \qquad \frac{d}{dt}\mathrm{div}^*(\mathbf{u}_{i,j,k}) \equiv 0, \quad \forall i, j, k.$$

There is a rich(-er) class of 3D consistent potentials which can be defined in a manner analogous to the two dimensional case. As an example, we define the three dimensional form of the symmetric potential (2.9), ϕ_1 as follows,

$$\begin{aligned} (\phi_1)_{i+\frac{1}{2}, j+\frac{1}{2}, k+\frac{1}{2}} &= \frac{1}{8}\left((F_1^y)_{i,j+\frac{1}{2},k} + (F_1^y)_{i+1,j+\frac{1}{2},k} + (F_1^y)_{i,j+\frac{1}{2},k+1} + (F_1^y)_{i+1,j+\frac{1}{2},k+1}\right) \\ &+ \frac{1}{8}\left((F_1^z)_{i,j,k+\frac{1}{2}} + (F_1^z)_{i+1,j,k+\frac{1}{2}} + (F_1^z)_{i,j+1,k+\frac{1}{2}} + (F_1^z)_{i+1,j+1,k+\frac{1}{2}}\right), \end{aligned}$$

where F_1^y, F_1^z are numerical fluxes consistent with the flux f_1 in the y- and z- directions respectively. The potentials ϕ_2, ϕ_3 can be similarly defined.

2.6. **Time stepping.** The constraint preserving schemes discussed so far are semi-discrete schemes and need to be coupled with suitable time integration routines. Consider, for example, the 2D potential-based scheme (2.7) at time level $t = t^n$,

$$(2.24) \qquad \frac{d}{dt}\mathbf{u}_{i,j}(t^n) = \mathbf{E}_{i,j}^n, \qquad \mathbf{E}_{i,j}^n := \left\{-\frac{1}{\Delta y}\delta_y\mu_x\phi_{i,j}^n, \frac{1}{\Delta x}\delta_x\mu_y\phi_{i,j}^n\right\}.$$

The simplest time stepping is the first-order accurate forward Euler scheme,

$$(2.25) \qquad \mathbf{u}_{i,j}^{n+1} = \mathbf{u}_{i,j}^n - \mathbf{E}_{i,j}^n,$$

where the time step Δt^n is limited by a suitable CFL condition. Second-order temporal accuracy can be obtained using a SSP Runge-Kutta method [14],

$$(2.26) \qquad \begin{aligned} \mathbf{u}_{i,j}^* &= \mathbf{u}_{i,j}^n - \Delta t^n\mathbf{E}_{i,j}^n, \\ \mathbf{u}_{i,j}^{**} &= \mathbf{u}_{i,j}^* - \Delta t^n\mathbf{E}_{i,j}^n, \\ \mathbf{u}_{i,j}^{n+1} &= \frac{1}{2}(\mathbf{u}_{i,j}^n + \mathbf{u}_{i,j}^{**}). \end{aligned}$$

An alternative first-order accurate genuinely multi-dimensional time stepping is the extended Lax-Friedrichs type time stepping,

$$
(2.27) \qquad \mathbf{u}_{i,j}^{n+1} = \frac{1}{8}(4\mathbf{u}_{i,j}^n + \mathbf{u}_{i+1,j}^n + \mathbf{u}_{i,j+1}^n + \mathbf{u}_{i-1,j}^n + \mathbf{u}_{i,j-1}^n) - \Delta t^n \mathbf{E}_{i,j}^n.
$$

3. Schemes for the Magnetic induction equation

The preceding description on constraint preserving schemes is very general. In order to provide some concrete stability estimates and perform numerical experiments, we focus on the two-dimensional form of the magnetic induction equations:

$$
(3.1) \qquad \begin{cases} (u_1)_t + (v_2 u_1 - v_1 u_2)_y = 0, \\ (u_2)_t - (v_2 u_1 - v_1 u_2)_x = 0, \end{cases}
$$

with the magnetic field $\mathbf{u} = (u_1, u_2)$ and a given velocity field $\mathbf{v} = (v_1, v_2)$.

In order to complete the divergence preserving potential based scheme (2.7), we need to specify numerical fluxes $F_{i+\frac{1}{2},j}^x, F_{i,j+\frac{1}{2}}^y$. The simplest available two point flux is the average flux:

$$
(3.2) \qquad F_{i+\frac{1}{2},j}^x = \frac{f_{i,j} + f_{i+1,j}}{2}, \quad F_{i,j+\frac{1}{2}}^y = \frac{f_{i,j} + f_{i,j+1}}{2},
$$

where $f(\mathbf{u}) = v_2 u_1 - v_1 u_2$. Using the above flux, together with the symmetric potential (2.9) results in the potential-based scheme:

$$
(3.3a) \qquad \begin{aligned} \frac{d}{dt}(u_1)_{i,j} &= -\frac{1}{2\Delta y}(\bar{f}_{i,j+1}^x - \bar{f}_{i,j-1}^x), \\ \frac{d}{dt}(u_2)_{i,j} &= \frac{1}{2\Delta x}(\bar{f}_{i+1,j}^y - \bar{f}_{i-1,j}^y), \end{aligned}
$$

where

$$
(3.3b) \qquad \bar{f}_{i,j}^x := \mu_x^2 f_{i,j} \equiv \frac{1}{4}(f_{i+1,j} + 2f_{i,j} + f_{i-1,j}), \quad \bar{f}_{i,j}^y := \mu_y^2 f_{i,j} \equiv \frac{1}{4}(f_{i,j+1} + 2f_{i,j} + f_{i,j-1}).
$$

The scheme (3.3a), which coincides with the *symmetric* scheme proposed in [30], preserves the discrete divergence,

$$
(3.4) \qquad \text{div}^*\big(\mathbf{u}_{i,j}(t)\big) = \text{div}^*\big(\mathbf{u}_{i,j}(0)\big), \qquad \text{div}^*(\mathbf{u}_{i,j}) := \frac{1}{\Delta x}\mu_y \delta_x(u_1)_{i,j} + \frac{1}{\Delta y}\mu_x \delta_y(u_2)_{i,j}.
$$

We will show that the potential-based symmetric scheme (3.3) is L^2-stable. Our proof highlights the role of (discrete) divergence-preserving. To motivate the numerical stability, we first provide the corresponding L^2 well-posedness statement in the continuous case.

Lemma 3.1. [11]. *Let $\mathbf{u}$ be the weak solution of the magnetic induction equations (3.1) subject to divergence free initial data, $\mathbf{u}_0 \in L^2(\mathbb{R}^2)$, and a convective velocity field $\mathbf{v} = (v_1, v_2) \in C^1(\mathbb{R}_+, \mathbb{R}^2)$. Then, $\mathbf{u}$ satisfies the apriori energy bound[1]*

$$
(3.5) \qquad \frac{d}{dt}\|\mathbf{u}\|_{L^2}^2 \lesssim \|\mathbf{v}\|_{C^1}\|\mathbf{u}\|_{L^2}^2.
$$

To verify (3.5) we follow [11]. Adding to (3.1) a zero source term which is proportional to vanishing divergence, we obtain,

$$
(3.6) \qquad \begin{aligned} (u_1)_t + (v_2 u_1 - v_1 u_2)_y &= -v_1(u_1)_x - v_1(u_2)_y, \\ (u_2)_t - (v_2 u_1 - v_1 u_2)_x &= -v_2(u_1)_x - v_2(u_2)_y, \end{aligned}
$$

---

[1]We use $X \lesssim Y$ to denote the estimate $X \leq CY$, where C is a constant which may depend on t but otherwise is independent of the solution, $\Delta x, \Delta y$ etc.

so that after straightforward simplifications, (3.1) recast into the *symmetric form,*

$$(3.7) \qquad \begin{aligned} (u_1)_t + v_1(u_1)_x + v_2(u_1)_y &= -(v_2)_y u_1 + (v_1)_y u_2, \\ (u_2)_t + v_1(u_2)_x + v_2(u_2)_y &= (v_2)_x u_1 - (v_1)_x u_2. \end{aligned}$$

The desired L^2-bound follows by applying the energy method for the symmetric form of the equations in (3.7) with bounded low-order term, $\|\mathbf{v}\|_{C^1} < \infty$.

We now turn to show that the potential-based symmetric scheme (3.3a) satisfies a discrete version of the L^2 energy estimate (3.5).

Lemma 3.2. *Let $\mathbf{u}_{i,j}$ be the solution of the semi-discrete potential based symmetric scheme (3.3) subject to divergence-free initial data $\mathrm{div}^*(\mathbf{u}(x_i, y_j, 0) \equiv 0$ and velocity field $\mathbf{v} \in C^1(\mathbb{R}_+, \mathbb{R}^2)$. Then, the following L^2-energy estimate holds,*

$$(3.8) \qquad \frac{d}{dt}\|\mathbf{u}\|_{L^2_\Delta}^2 \lesssim \|\mathbf{v}\|_{C^1}\|\mathbf{u}\|_{L^2_\Delta}^2, \qquad \|\mathbf{u}\|_{L^2_\Delta}^2 := \Delta x \Delta y \sum_{i,j}(u_1)_{i,j}^2 + (u_2)_{i,j}^2.$$

Proof. We mimic the proof of the continuous estimate (3.5). We begin by writing the discrete divergence div^* in the form

$$\mathrm{div}^*(\mathbf{u}_{i,j}) = \frac{1}{2\Delta x}\Big((\bar{u}_1^y)_{i+1,j} - (\bar{u}_1^y)_{i-1,j}\Big) + \frac{1}{2\Delta y}\Big((\bar{u}_2^x)_{i,j+1} - (\bar{u}_2^x)_{i,j-1}\Big),$$

where $\bar{u}^x$ and $\bar{u}^y$ are the averages (3.3b). The discrete divergence preservation (3.4) tells us that $\mathrm{div}^*(\mathbf{u}_{i,j}) \equiv 0$: adding a multiple of this vanishing divergence as a discrete source term to (3.3a) yields a discrete analogue of (3.6)),

$$(3.9) \qquad \begin{aligned} \frac{d}{dt}(u_1)_{i,j} &= -D_y^0 \bar{f}_{i,j}^x - (v_1)_{i,j}D_x^0(\bar{u}_1^y)_{i,j} - (v_1)_{i,j}D_y^0\bar{u}_{2,i,j}^x, \\ \frac{d}{dt}(u_2)_{i,j} &= D_x^0 \bar{f}_{i,j}^y - (v_2)_{i,j}D_x^0(\bar{u}_1^y)_{i,j} - (v_2)_{i,j}D_y^0(\bar{u}_2^x)_{i,j}. \end{aligned}$$

Substituting the explicit form of $f = v_2 u_1 - u_2 v_1$ in (3.9), one obtains after straightforward manipulations, the following discrete version of the *symmetric form* of the equations in (3.7),

$$(3.10) \qquad \begin{aligned} \frac{d}{dt}(u_1)_{i,j} &= -(v_1)_{i,j}D_x^0(\bar{u}_1^y)_{i,j} - (v_2)_{i,j}D_y^0(\bar{u}_1^x)_{i,j} - \frac{1}{2}\Big(D_y^+(\bar{v}_2^x)_{i,j}(\bar{u}_1^x)_{i,j+1} + D_y^-(\bar{v}_2^x)_{i,j}(\bar{u}_1^x)_{i,j-1}\Big) \\ &\quad + \frac{1}{2}\Big(D_y^+(\bar{v}_1^x)_{i,j}(\bar{u}_2^x)_{i,j+1} + D_y^-(\bar{v}_1^x)_{i,j}(\bar{u}_2^x)_{i,j-1}\Big), \\ \frac{d}{dt}(u_2)_{i,j} &= -(v_1)_{i,j}D_x^0(\bar{u}_2^y)_{i,j} - (v_2)_{i,j}D_y^0(\bar{u}_2^x)_{i,j} + \frac{1}{2}\Big(D_x^+(\bar{v}_2^y)_{i,j}(\bar{u}_1^y)_{i+1,j} + D_x^-(\bar{v}_2^y)_{i,j}(\bar{u}_1^y)_{i,j-1}\Big) \\ &\quad - \frac{1}{2}\Big(D_x^+(\bar{v}_1^y)_{i,j}(\bar{u}_2^y)_{i,j+1} + D_x^-(\bar{v}_1^y)_{i,j}(\bar{u}_2^y)_{i,j-1}\Big). \end{aligned}$$

We conclude with energy method: summing by parts the first equation in (3.10) against $\Delta x \Delta y (u_1)_{i,j}$ and the second equation against $\Delta x \Delta y (u_2)_{i,j}$ and using Cauchy's inequality, we obtain the L^2 energy estimate (3.8). $\square$

Note that preserving the discrete divergence (3.4) plays a crucial role in the L^2-stability of the potential-based scheme (3.3). Since the scheme is based on centered stencil it is unconditionally *unstable*, when combined with the forward Euler or second-order Runge Kutta (RK) time stepping (2.25), (2.26). Stability can be achieved by using higher-order (≥ 3) RK time stepping, e.g., [27]. Alternatively, a standard way to stabilize centered-based schemes is achieved by adding numerical diffusion (2.4). A simple Rusanov type numerical diffusion operator, (2.5), is used to modify the numerical fluxes (3.2), yielding the viscous numerical fluxes,

$$(3.11) \qquad \begin{aligned} F_{i+\frac{1}{2},j}^x &= F^x(\mathbf{u}_{i,j}, \mathbf{u}_{i+1,j}) = \frac{1}{2}(f_{i,j} + f_{i+1,j}) + \max\{|(v_1)_{i,j}|, |(v_1)_{i+1,j}|\}\big((u_2)_{i+1,j} - (u_2)_{i,j}\big) \\ F_{i,j+\frac{1}{2}}^y &= F^y(\mathbf{u}_{i,j}, \mathbf{u}_{i+1,j}) = \frac{1}{2}(f_{i,j} + f_{i,j+1}) - \max\{|(v_2)_{i,j}|, |(v_2)_{i,j+1}|\}\big((u_1)_{i,j+1} - (u_1)_{i,j}\big). \end{aligned}$$

The diffusive terms involve the maximum wave speeds in each direction. Other diffusion operators, like the standard upwind diffusion, can also be used. Once the diffusive numerical fluxes are set, one can define the

corresponding numerical potential and complete the potential-based scheme (2.7). We are unable, however, to prove that the scheme (2.7) with numerical diffusion (like in (3.11)) is L^2-energy stable. Nevertheless, numerical experiments in the sequel suggest that the potential-based scheme with numerical diffusion is energy stable.

4. NUMERICAL EXPERIMENTS

We test the constraint preserving schemes for the magnetic induction equation (3.1) in this section. The following four schemes are considered:

RUS   Standard first-order Rusanov scheme, (2.3),(3.11).
CPR   Constraint preserving scheme (2.7) with Rusanov flux.
CPR2   Second-order (both space and time) constraint preserving scheme, (2.14), based on Rusanov flux (2.5).
CPS   Constraint preserving symmetric scheme (3.3a) with the Runge-Kutta time stepping.

All schemes are updated in time with a CFL number of 0.45.

4.1. **Numerical experiment #1: rotating hump.** This test case is a benchmark for testing schemes for multi-dimensional advection [30, 11]. We consider the two dimensional magnetic induction equation (3.1) with the velocity field $(v_1, v_2) = (-y, x)$. The exact solution can be calculated as

$$(4.1) \qquad \mathbf{u}(x, y, t) = R(t)\mathbf{u}_0(R(-t)(x, y)),$$

where $R(t)$ is a rotation matrix with angle t.

We consider the divergence free initial data:

$$(4.2) \qquad \mathbf{u}_0(x, y) = 4 \begin{pmatrix} -y \\ x - \frac{1}{2} \end{pmatrix} e^{-20\left((x - \frac{1}{2})^2 + y^2\right)},$$

and the computational domain $[-1, 1] \times [-1, 1]$. The exact solution (4.1) is a smooth hump (centered at $(\frac{1}{2}, 0)$) rotating about the origin and completing one rotation in time $t = 2\pi$. Non-reflecting Neumann type boundary conditions are used.

The approximate solutions at time $t = 2\pi$ on a 100×100 mesh are shown in figure 1. We show the norm $\|\mathbf{u}\| = \sqrt{u_1^2 + u_2^2}$ with four different schemes. The constraint preserving schemes are based on the symmetric potential (2.9). The figure shows that the standard RUS scheme does a poor job of approximating the rotating hump. The magnitude of the hump is smeared considerably and the shape is distorted. Unphysical waves are also generated. In sharp contrast, the constraint preserving schemes approximate the solution quite well. The first-order CPR scheme smears the solution somewhat (note different scales in the figures) but the shape is still maintained. The second-order CPR2 and the CPS schemes resolve the solution very sharply. The smearing is reduced considerably and the shape is maintained. The results suggest a strong connection between divergence preservation and the numerical performance. This link is quantified in Table 1 where we tabulate the discrete divergence div^* (2.8a) in L^2, generated with all the four schemes at time $t = 2\pi$. Note that since the initial data is divergence free, the exact divergence will be zero at all times.

Grid size	RUS	CPR	$CPR2$	CPS
50/50	2.15e-1	6.07e-7	$1.27e - 7$	$7.0e - 7$
100/100	8.15e-2	3.04e-9	$2.9e - 8$	$1.5e - 10$
200/200	2.2e+3	5.34e-12	$2.88e - 14$	$2.8e - 14$
400/400	diverges	5.53e-14	$7.1e - 15$	$7.8e - 15$

TABLE 1. Absolute errors in L^2 for $\|\mathrm{div}^*\|$ at time $t = 2\pi$ for the rotating hump with four different schemes.

Table 1 shows that the standard RUS scheme generates divergence errors of the order of the truncation error on coarse meshes. However, the scheme is unstable on fine meshes and crashes on a 400×400 mesh. The blow up of RUS scheme based on 400×400 mesh points was preceded by a large increase in the divergence, indicating
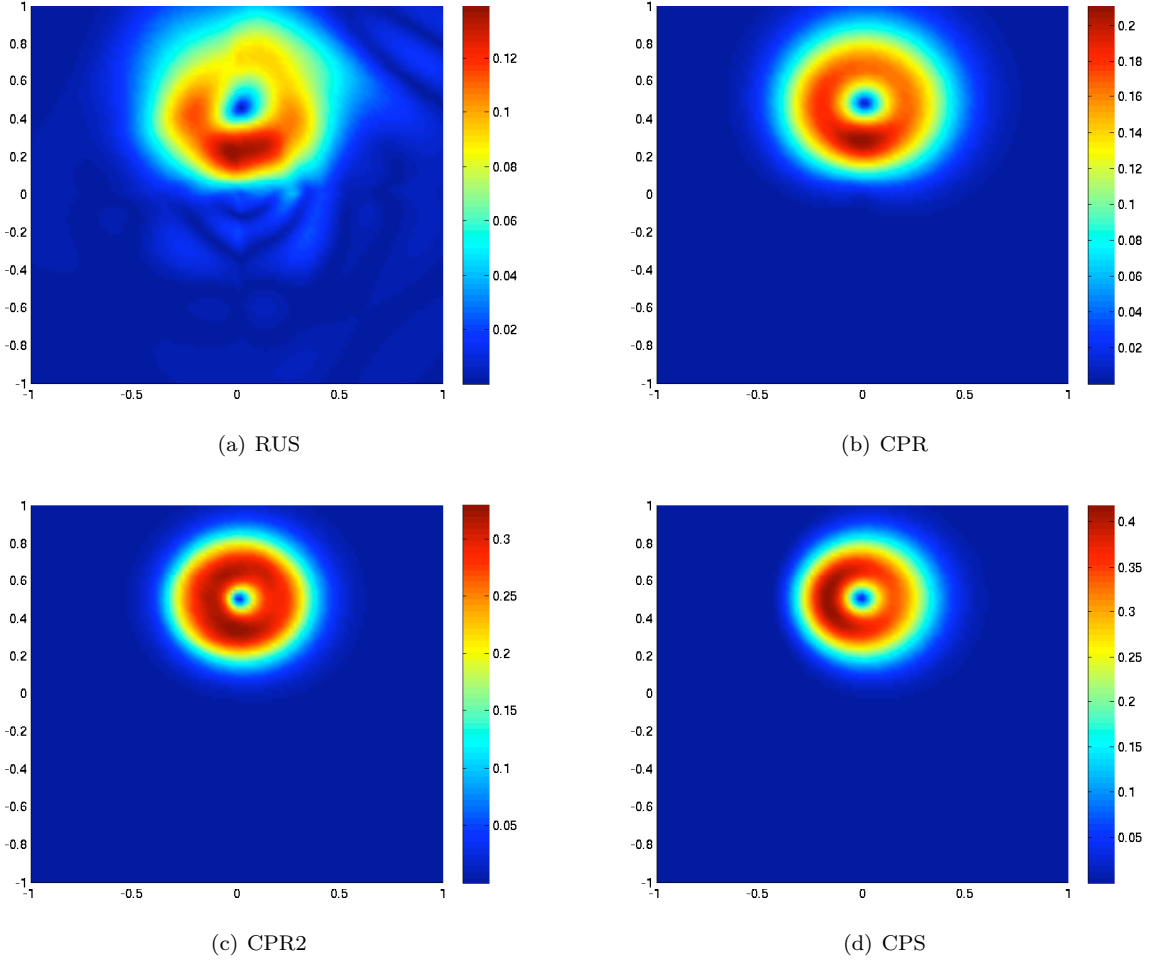
FIGURE 1. $\|\mathbf{u}\|$ at time $t = 2\pi$ in the rotating hump experiment with four different schemes on a 100×100 mesh.

a possible connection between the two. The constraint preserving schemes result in very small divergence errors, mostly due to boundary effects (no special divergence cleaning is applied at the boundary). The errors on coarse meshes are very small and converge to zero quite rapidly. As expected, the errors are of the order of machine precision on fine meshes.

The operator div^* is a particular discrete form of the divergence operator. We have shown that the constraint preserving scheme (2.7) preserves this particular form of divergence. A natural question is what happens when a different form of discrete divergence is used. We consider the standard centered discrete divergence operator,

$$\mathrm{div}(\mathbf{u}_{i,j}) = D_x^0(u_1)_{i,j} + D_y^0(u_2)_{i,j}.$$

A simple calculation shows that div and div^* differ by $\mathcal{O}(\Delta x^2 + \Delta y^2)$. Therefore, preserving div^* would only imply that errors in div behave like the square of the truncation error. This issue is explored quantitatively and the results are shown in Table 2. The table shows that the errors in the standard divergence div, generated by the constraint preserving schemes, are low and are consistently lower than the expected square of the truncation error. Consequently, we conclude that using a divergence preserving scheme will lead to lower errors for other discrete forms of divergence.

Grid size	RUS	CPR	$CPR2$	CPS
50/50	2.16e-1	1.48e-2	$1.43e-2$	$1.8e-2$
100/100	8.29e-2	3.2e-3	$1.32e-3$	$1.6e-3$
200/200	1.99e+3	6.26e-4	$6.7e-5$	$2.0e-4$
400/400	blow-up	1.67e-4	$4.4e-5$	$5.6e-6$

TABLE 2. Absolute errors in L^2 for $\|\text{div}\|$ at time $t = 2\pi$ for the rotating hump with four different schemes.

In the above discussion, the divergence preserving schemes were based on the symmetric potential (2.9). We use all the four potentials described in section 2 with the first-order CPR scheme and show $\|\mathbf{u}\|$ for the approximate solution at time $t = \pi/4$ on a 100×100 mesh in figure 2. The figure clearly shows that different

(a) Symmetric

(b) StagSym

(c) Diagonal

(d) Mixed
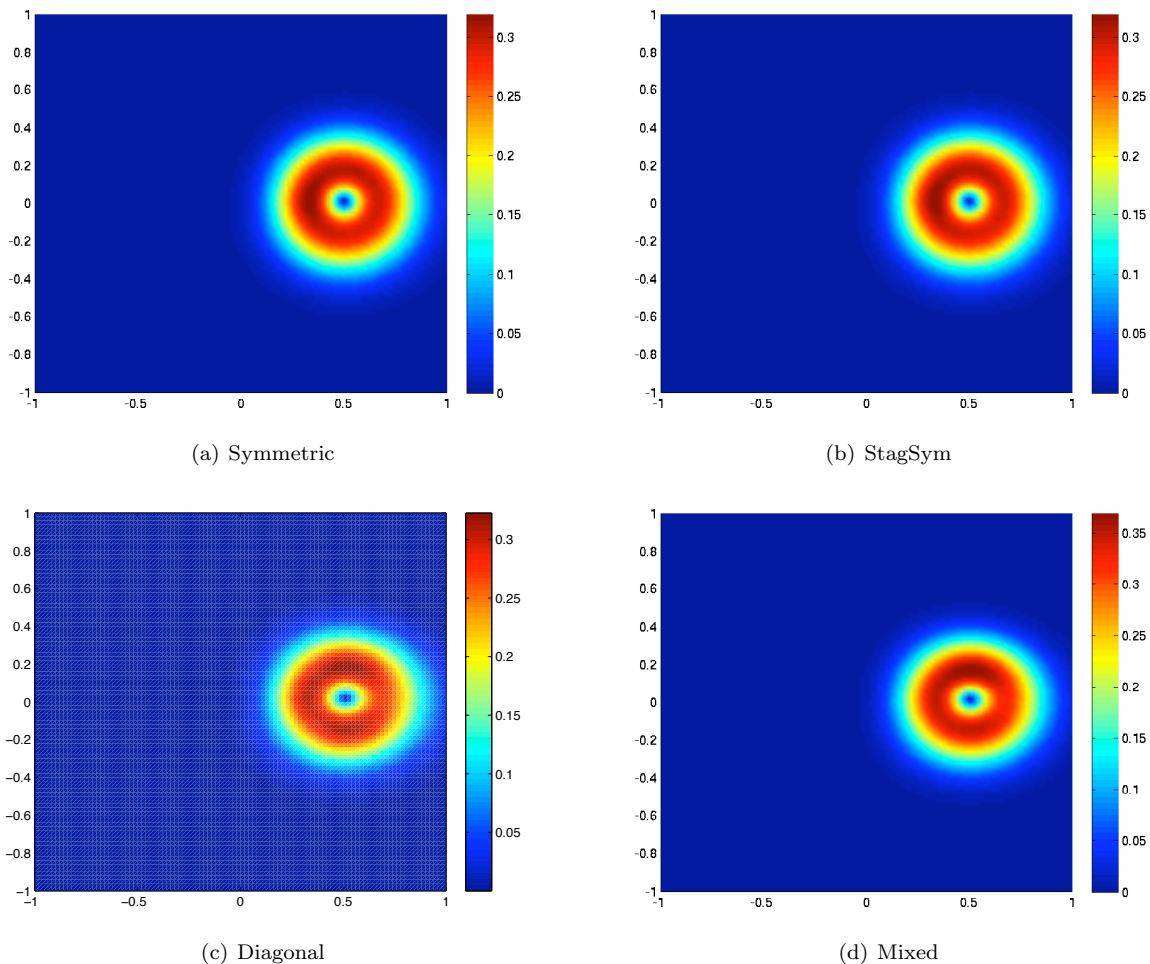
FIGURE 2. Rotating Hump: $\|\mathbf{u}\|$ at time $t = \pi/4$ on a 100×100 mesh with the CPR scheme and different potentials.

choices of potential resulted in very similar numerical approximations. This was also seen in other experiments, indicating the robustness of our approach with respect to varying choices of potentials. However, there were some boundary instabilities for the diagonal potential when long time scales were considered. This fact requires careful investigation in the future.

4.2. **Numerical experiment #2: discontinuous test case.** The rotating hump involved smooth solutions. However, we can expect discontinuous solutions (particularly in MHD models). We test the constraint preserving scheme on a numerical experiment involving discontinuities in the solution. The initial data is given by, [11],

$$u_1^0(x,y) = u_2^0(x,y) = \begin{cases} 2 & \text{if } x > y, \\ 0 & \text{otherwise.} \end{cases}$$

and the velocity field is a constant $\mathbf{v} = (1,2)$. The exact solution is the initial discontinuity moving along the diagonal,

$$\mathbf{u}(x,y,t) = \mathbf{u}^0(x-t, y-2t).$$

We consider the computational domain $[-2,2] \times [-2,2]$ and use extrapolated Neumann boundary conditions. A one dimensional slice (at $y = 0.0$) of the solution component u_1 computed with the RUS, CPR and CPR2 schemes at time $t = 0.5$ on a 100×100 mesh is shown in figure 3. The figure shows that the standard RUS
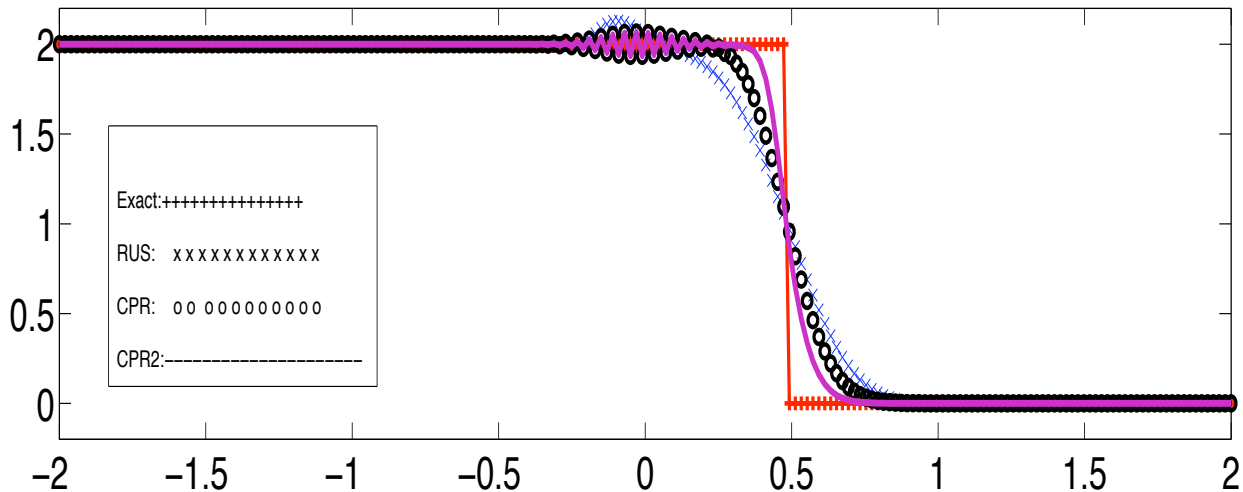
FIGURE 3. Numerical experiment 2: $u_1(x,0,0.5)$ on a 100×100 mesh with different schemes.

scheme leads to a large overshoot. This fact was first observed in [11]. Furthermore, the discontinuity is smeared to a large extent. The CPR scheme reduces the overshoot considerably and resolves the discontinuity with very little smearing. However there are small amplitude oscillations, showing that the constraint preserving scheme is not necessarily total-variation diminishing (TVD), although the exact solution in this particular experiment is TVD. The second-order CPR2 scheme resolves the discontinuity more sharply and the oscillations are also reduced. The results show that the constraint preserving schemes are not diffusive enough in this case. A simple method for increasing the diffusion without affecting the constraint preserving abilities is to use the genuinely multi-dimensional Lax-Friedrichs type time-stepping (2.27) with the CPR scheme. We term this scheme and its second-order (in space) version as aCPR and aCPR2 scheme respectively. The results are shown in figure 4. The aCPR scheme removes the oscillations, at the cost of smearing the discontinuity. The spatially second-order aCPR2 scheme captures the discontinuity more sharply and without any noticeable oscillations. This alternative time stepping provides a simple recipe of modifying the constraint preserving schemes to eliminate unphysical oscillations.

Remark 4.1. *The potential based scheme (2.7) is slightly more expensive than its building block, the standard finite volume scheme (2.3). However, the overall cost is still quite low. The simplicity and generality of this approach renders it considerably cheaper and easier to implement than competing constraint preserving frameworks. The extra computational cost is justified by the considerable increase in stability and resolution.*
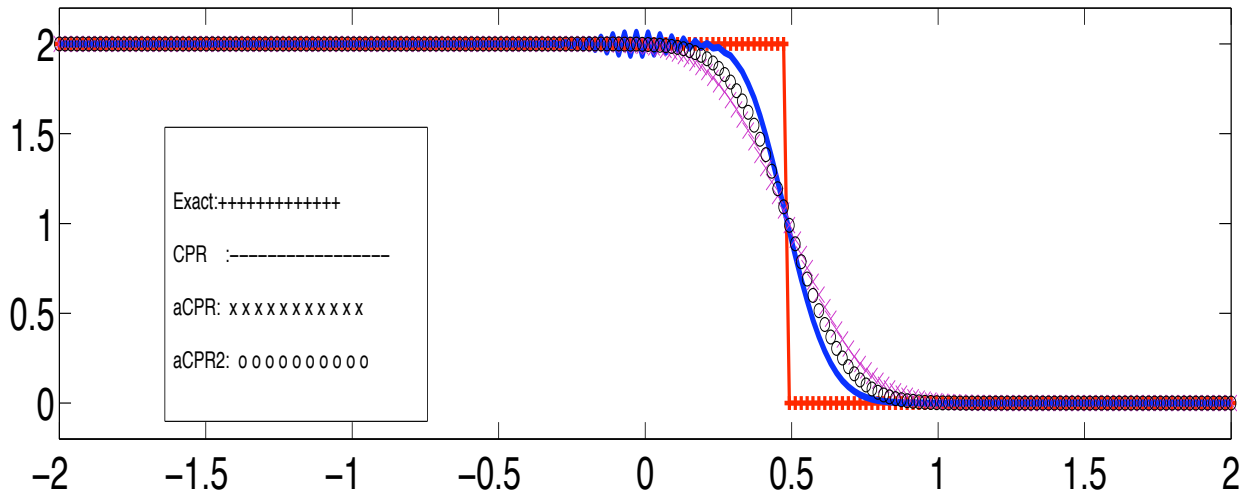
FIGURE 4. Numerical experiment 2: $u_1(x, 0, 0.5)$ on a 100×100 mesh with different schemes.

5. CONCLUSION

Evolution equations (1.1) with an intrinsic constraint (1.2) are considered. Examples include the divergence preserving equations (1.3) and the curl preserving equations (1.8). Standard finite volume schemes (2.3) do not necessarily preserve discrete versions of the constraint and may be unstable.

We design finite volume schemes for (1.1) that preserve discrete forms of the constraint (1.2). The schemes are based on *vertex centered numerical potentials*. The resulting scheme is genuinely multi-dimensional and constraint preserving. The class of potential based schemes is very rich. Potential based schemes are presented for both the divergence preserving equation (1.3) and curl preserving equation (1.8). Constraint preserving schemes for the equations with viscosity (1.7) are also proposed. Second-order accuracy is obtained by employing non-oscillatory piecewise polynomial reconstructions.

The magnetic induction equations in two dimensions (3.1) are considered in detail. A divergence preserving potential based scheme is shown to be L^2-stable. Numerical experiments demonstrating the robustness and computational efficiency of the constraint preserving schemes are presented. They show that the schemes perform considerably better than standard schemes.

The main advantage of this new approach is its simplicity and generality. This paper is the first in a series. Subsequent papers include ones describing potential based genuinely multi-dimensional schemes for systems of conservation laws [19] and divergence preserving schemes for the ideal MHD equations [20]. Extending the potential based schemes to higher than second order accuracy and to unstructured grids will be considered in future papers.

REFERENCES

[1] R. Artebrant and M.Torrilhon. Increasing the accuracy of local divergence preserving schemes for MHD. *J. Comp. Phys.*, 227 (6), 3405-3427, 2008.

[2] J. Bálbas , E. Tadmor. Non-oscillatory central schemes for one- and two-dimensional MHD equations. II: high-order semi-discrete schemes. *SIAM J. Sci. Comput.,* 28 (2006) 533-560.

[3] J. Bálbas , E. Tadmor and C. C. Wu. Non-oscillatory central schemes for one and two-dimensional magnetohydrodynamics I. *J. Comp. Phys.,* 201 (1), 261-285, 2004.

[4] D. S. Balsara and D. Spicer. A staggered mesh algorithm using high order Godunov fluxes to ensure solenoidal magnetic fields in magnetohydrodynamic simulations. *J. Comp. Phys.*, 149(2):270-292, 1999.

[5] J. B. Bell, P. Colella and H. M. Glaz. A second-order projection method for the incompressible Navier-Stokes equations. *J. Comp. Phys.*, 85, 257-283, 1989.

[6] J. U. Brackbill and D. C. Barnes. The effect of nonzero Div$B$ on the numerical solution of the magnetohydrodynamic equations. *J. Comp. Phys.*, 35:426-430, 1980.

[7] A. J. Chorin. Numerical solutions of the Navier-Stokes equations. *Math. Comp.*, 22, 745-762, 1968.

[8] W. Dai and P. R. Woodward. A simple finite difference scheme for multi-dimensional magnetohydrodynamic equations. *J. Comp. Phys.*, 142(2):331-369, 1998.

[9] C. Evans and J. F. Hawley. Simulation of magnetohydrodynamic flow: a constrained transport method. *Astrophys. J.*, 332:659, 1998.

[10] A. J. Font. Numerical hydrodynamics in general relativity. *Living Rev. Relativ.* 2003 (6), 87 pages.

[11] F. Fuchs, K. H. Karlsen, S. Mishra and N.H. Risebro. Stable upwind schemes for the Magnetic Induction equation. *M2AN Math. Model. Num. Anal.,* to appear, 2009.

[12] F. Fuchs, A. D. McMurry, S. Mishra, N. H. Risebro and K. Waagan. Approximate Riemann solver based high order finite volume schemes for the Godunov-Powell form of the ideal MHD equations in multi dimensions. *Preprint,* 2009.

[13] S. K. Godunov. The symmetric form of magnetohydrodynamics equation. *Num. Meth. Mech. Cont. Media*, 1:26-34, 1972.

[14] S. Gottlieb, C. W. Shu and E. Tadmor. High order time discretizations with strong stability property. *SIAM. Review,* 43, 2001, 89 - 112.

[15] A. Harten, B. Engquist, S. Osher and S. R. Chakravarty. Uniformly high order accurate essentially non-oscillatory schemes. *J. Comput. Phys.*, 1987, 231-303.

[16] R. Jeltsch and M. Torrilhon. On curl preserving finite volume discretizations of the shallow water equations. *BIT*, 46, 2006, suppl.

[17] A. Kurganov and E. Tadmor. New high resolution central schemes for non-linear conservation laws and convection-diffusion equations. *J. Comput. Phys*, 160(1), 241-282, 2000.

[18] R. J. LeVeque. Finite volume methods for hyperbolic problems. *Cambridge university press,* Cambridge, 2002.

[19] S. Mishra and E. Tadmor. Constraint preserving schemes using potential-based fluxes II. Genuinely multi-dimensional central schemes for systems of conservation laws. *Preprint.*

[20] S. Mishra and E. Tadmor. Constraint preserving schemes using potential-based fluxes III. Genuinely multi-dimensional schemes for MHD equations. *Preprint.*

[21] K. W. Morton and P. L. Roe. Vorticity preserving Lax-Wendroff type schemes for the system wave equation. *SIAM. J. Sci. Comput.,* 23 (1), 2001, 170-192.

[22] K. G. Powell. An approximate Riemann solver for magneto-hydro dynamics (that works in more than one space dimension). Technical report, 94 -24, ICASE, Langley, VA, 1994.

[23] K. G. Powell, P. L. Roe. T. J. Linde, T . I. Gombosi and D . L. De zeeuw, A solution adaptive upwind scheme for ideal MHD. J. Comp. Phys, 154(2), 284 - 309, 1999

[24] D. S. Ryu, F. Miniati, T. W. Jones and A. Frank. A divergence free upwind code for multidimensional magnetohydrodynamic flows. *Astrophys. J.*, 509(1):244-255, 1998.

[25] C. W. Shu and S. Osher. Efficient implementation of essentially non-oscillatory schemes - II, *J. Comput. Phys.*, 83, 1989, 32 - 78.

[26] E. Tadmor. Numerical viscosity and entropy conditions for conservative difference schemes. *Math. Comp.*, 43 (168), 369 -381, 1984.

[27] E. Tadmor. From semi-discrete to fully discrete: stability of Runge-Kutta schemes by the energy method. II. in "Collected Lectures on the Preservation of Stability under Discretization", Proc. in Applied Mathematics (D. Estep and S. Tavener, eds.) 109, SIAM 2002, 25-49.

[28] E. Tadmor. Approximate solutions of nonlinear conservation laws. *Advanced Numerical approximations of Nonlinear Hyperbolic equations, A. Quarteroi ed.*, Lecture notes in Mathematics, Springer Verlag (1998), 1-149.

[29] M. Torrilhon. Locally divergence preserving upwind finite volume schemes for magneto-hydro dynamics. *SIAM. J. Sci. Comp.*, 26 (4), 1166-1191, 2005.

[30] M. Torrilhon and M. Fey. Constraint-preserving upwind methods for multidimensional advection equations. *SIAM. J. Num. Anal.*, 42(4):1694-1728, 2004.

[31] G. Toth. The Div$B = 0$ constraint in shock capturing magnetohydrodynamics codes. *J. Comp. Phys.*,161:605-652, 2000.

(Siddhartha Mishra)
SAM, D-MATH
ETH Zürich
HG. G. 57.2, Rämistrasse 101, Zürich, Switzerland
   E-mail address: smishra@sam.math.ethz.ch

(Eitan Tadmor)
Department of Mathematics
Center of Scientific Computation and Mathematical Modeling (CSCAMM)
Institute for Physical sciences and Technology (IPST)
University of Maryland
MD 20742-4015, USA
   E-mail address: tadmor@cscamm.umd.edu

Research Reports